

HIGH-RESOLUTION MULTIBEAM SONAR MAPPING WITH THE AUTONOMOUS BENTHIC EXPLORER (ABE)

M. V. Jakuba
MIT/WHOI Joint Program
jakuba@mit.edu

D. R. Yoerger
Woods Hole Oceanographic Institution
dyoerger@whoi.edu

1 Abstract

In two recent deployments the Autonomous Benthic Explorer (ABE) of the Woods Hole Oceanographic Institution (WHOI) collected high-resolution multibeam sonar bathymetry of Explorer Ridge (July 2002) and the Lost City vent site (May 2003). A Simrad Mesotech SM 2000 multibeam sonar has been fully integrated into the vehicle for this purpose. The challenging topography of the Lost City site demanded careful AUV survey planning, but also afforded the opportunity to try new survey techniques, particularly side-looking surveys along steep slopes. The quality of post-processed navigation has been improved with the addition of a model-based smoother. To aid in processing the large volume of sonar data generated during surveys, we have developed a high-level user interface in the form of a MATLAB GUI that allows users to inspect sonar images and the corresponding bathymetry concurrently. Using these techniques, bathymetric maps gridded on 2 m regular grids are visually free of trackline artifacts.

2 Introduction

The Autonomous Benthic Explorer (ABE) of the Woods Hole Oceanographic Institution (WHOI) is an Autonomous Underwater Vehicle (AUV) that supports basic scientific survey of the seafloor and the near-bottom water column. Two recent deployments (May 2003, Lost City; July 2002, Explorer Ridge) focused on the collection of high-resolution multibeam

sonar bathymetry. ABE's design, which enables it to climb vertically, hover, and reverse, makes it well-suited to collecting sonar bathymetry in areas with rough topography, a task which requires a maneuverable vehicle capable of maintaining a near constant altitude above bottom [6]. To collect sonar bathymetry, ABE is equipped with a 80-element Simrad SM 2000 200 kHz multibeam sonar [3]. This system is now fully integrated into the vehicle, with a dedicated PC104 stack located inside the main electronics housing. In addition to bathymetry from the SM 2000 system and an Imagenix pencil beam scanning-head sonar, ABE collects co-registered magnetometric, CTD, optical backscatter, and redox potential data. During ABE's missions, the host ship was generally free to perform other research activities.

3 SM 2000 on ABE

As sold by Kongsberg Simrad Mesotech, the SM 2000 unit comes with a Windows-based topside PC. The topside PC manages telemetry, unpacking of the data stream from the head, beamforming, bottom detection, the logging of raw and processed data, and real-time display. Size and interface incompatibilities precluded the possibility of integrating the topside unit into ABE. Instead, a dedicated PC-104 stack within the main electronics housing communicates directly with the sonar head at 460 kbaud, sending commands and logging data as necessary. The data returned by the head (amplified and digitized in-phase and

quadrature sound pressure from each element) are logged directly. All unpacking and processing (including beamforming) are done on deck after recovery on a separate machine.

3.1 Hardware

The Simrad SM 2000 multibeam sonar installed on ABE transmits at 200 kHz with a 1.5° by 120° transmit beam and 80 receiving elements arranged in a 120° arc [3]. The transmitter and receiver units are separate. The lower hull of ABE was modified to accommodate the downward facing SM 2000 transducers. Both the receive and transmit units are mounted on a frame that can be rotated manually to point to starboard at up to 60° from vertical, in 15° increments. Flotation was added as necessary to compensate for the extra weight of the transducers and maintain neutral buoyancy.



Figure 1: SM 2000 hardware on ABE as installed during the Explorer Ridge expedition. The transducers are visible on the underside of the vehicle. The SM 2000 transducers have since been mounted on a rotating frame that allows a static rotation of up to 60° to starboard. The frame is faired into the lower hull and all additional flotation has been moved inside the hulls.

3.2 Vehicle interface

Figure 2 shows how SM 2000 data is recorded on ABE. A dedicated PC-104 stack programmed by WHOI commands the SM 2000 transmitter to ping once every 2 s (red line). Ping rates can be programmed faster or slower depending on sonar settings and mission profile, but ultimately the data transfer rate out of the sonar head limits ping rate. Data are collected at the SM 2000 receiver for a predetermined duration, and sent to the logger upon reception of the next ping command (blue line). Collected data are timestamped by the logger and recorded on a dedicated hard disk. Simultaneously, a “ping reception time stamp” is sent to the main ABE PC-104 stack, timestamped with ABE time and recorded (green line). The clocks on each stack are synchronized before each dive, but this method of dual timestamping ensures that all data can be co-registered with vehicle position/attitude, regardless drift between the time-bases of the stacks. It also minimizes the amount of information traveling between the two stacks.

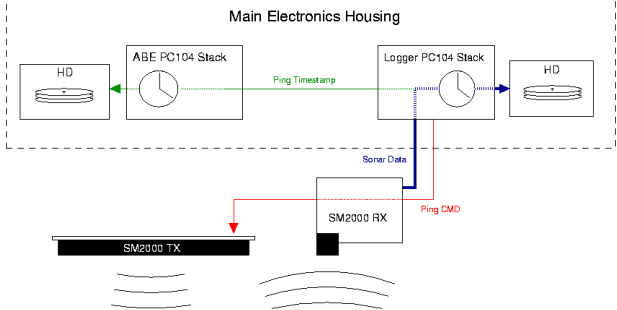


Figure 2: SM 2000 data recording schematic.

4 Survey Methodology

ABE collected high-resolution multibeam bathymetry of a portion of the Explorer Ridge ($49^\circ 46' \text{ N}$, $130^\circ 16' \text{ W}$) over the course of 5 dives from July 2–9, 2002, and of the Lost City vent site (30° N , Mid-Atlantic Ridge) over the course of 16 dives from April 27–May 15, 2003. Careful survey

design, from the placement of LBL transponders through trackline planning, is crucial to successful map-making. Survey parameters, particularly trackline spacing and bottom-following altitude, should be chosen such that the bathymetric sonar resolution is on par with navigational accuracy (Section 8).

At the Explorer Ridge site, ABE followed the generic, “lawn mower-like” survey lines shown in Figure 4. Regular grid surveys are appropriate where the vehicle’s safety will not be compromised, where the vehicle will not have to spend much of its time conducting energy-consuming climbs, and where the quality of sonar returns will not be compromised. The trajectory followed by dive ABE-84 over Lost City (shown in blue in Figure 5) covers the remarkably flat summit in a similar regular grid. A portion of the dive was also devoted to surveying the vent field in detail. The Lost City vent site is characterized by carbonate towers 10s of meters tall. A tightly-spaced survey along perpendicular tracklines over the vent site ensured that the shadows of these structures did not produce holes in coverage.

In contrast, the steeply sloped southern face of the Lost City vent site evident in Figure 5 afforded the opportunity to try new survey techniques, particularly side-looking surveys planned along contour lines.

The first several dives at Lost City were planned conservatively using multibeam bathymetry collected from the ship’s SeaBeam bathymetric sonar system. ABE excels at cliff-climbing [5] and its 30° forward looking altimeter cannot resolve objects on its flanks, thus all surveys over unmapped territory were designed to ensure ABE flew across rather than along contours.¹ ABE-80 was the first exploratory dive at Lost City. Shown in black in Figure 5, the survey was designed to minimize risk to the vehicle and to localize the cliff edge, which was poorly resolved in the SeaBeam bathymetry. As an additional safety measure, the maximum allowed depth was set to just below the cliff edge. Rather than risk the vehicle bottom-following over uncertain terrain, we relied on the long range of the multibeam (set to 200 m on this

¹In principle, data from either the Imagenix scanning-head sonar or the SM 2000 multibeam sonar could be incorporated into the obstacle-avoidance and bottom-following algorithms

dive) to collect bathymetry. Although this dive did not completely resolve the cliff edge (stiff south currents prevented the vehicle from finishing the north-going legs of the survey before timing out), it did provide the first high-resolution bathymetry of the Lost City site.

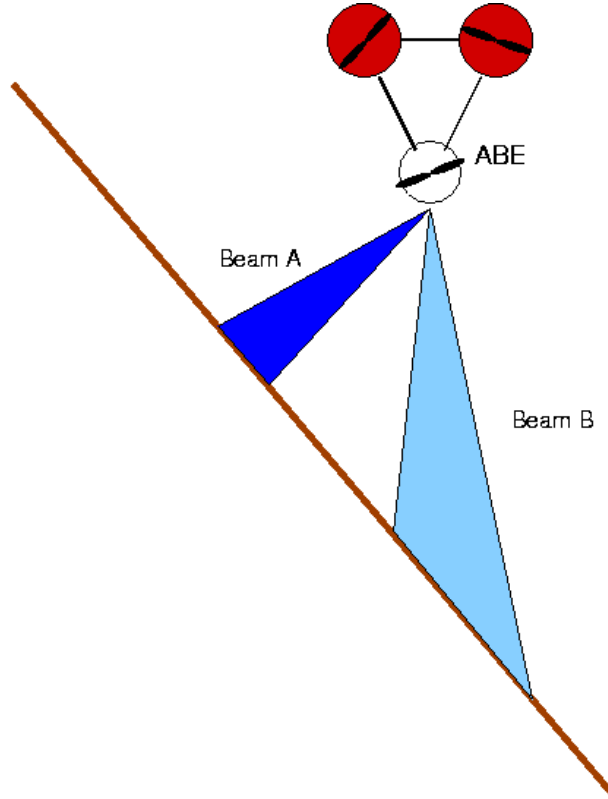


Figure 3: Sonar geometry for a survey along a steep slope. The resolution of side-looking beams (A) is improved over down-looking beams (B).

ABE surveyed the steeply sloped southern face of the site by driving along tracklines roughly aligned with topographic contours. During these surveys the SM 2000 was pointed either directly down or to starboard at 30°. While transverse cliff climbing is a safe mode of operation for ABE, it requires substantially more energy than flying straight-and-level. As higher resolution bathymetry of the top of the massif

became available, our confidence in the low resolution SeaBeam bathymetry increased and we were able to plan contour-following surveys along the southern slope. Tracklines from ABE-90, a representative survey of this type, are shown in Figure 5. To keep ABE flying level, the maximum depth on each trackline was set such that the bottom remained in range of the multibeam without requiring the vehicle to bottom-follow except over unexpected high areas.

Side-looking surveys along slopes require the vehicle to make return trips in the opposite direction during which the sonar will look away from the face and into open water. Despite the implication that roughly half of such a survey generates no bathymetry, the sonar returns collected during the productive half are of higher quality than they would be if the sonar were oriented vertically. The physical area of the bottom insonified by each beam increases as the angle of incidence is decreased from 90° , thus reducing the resolution of that beam, as illustrated in Figure 3. The strength of the return is also compromised at low angles of incidence, increasing the possibility of false detection from a side lobe with more favorable geometry.

5 Kalman Smoother-based Navigation Post-Processing

While underway, ABE generates navigation fixes by interrogating a long baseline (LBL) transponder net and measuring the round trip travel times to each beacon. Accepted travel times are used to compute the fix in a least squares sense. Between fixes, the vehicle dead-reckons based on measured heading and commanded thrust. This procedure is sufficient for real-time navigation; however it does not provide fixes of sufficient accuracy to generate bathymetry of a precision commensurate with that of the images generated by the multibeam sonar. For a typical survey (50 m above bottom, 2 s ping rate, 0.5 m/s flight speed, 128 beams spaced evenly over a 90° swath angle) the multibeam sonar provides a resolution of roughly 1 m horizontally and 0.25 --0.5 m vertically. The accuracy of our post-processed LBL-based navi-

gation is approaching this figure.

To improve the quality of navigation between LBL fixes and to reduce the noise inherent in LBL navigation, we filter the real-time computed LBL fixes through a Kalman smoother-based algorithm. A Kalman filter mixes measurements of a process with predictions from a model of that process in proportion to the covariances associated with each. A smoother has the additional advantage that all measurements, past and future, are used in the estimation. Our method is a straightforward application of the RTS algorithm (see for example [4]).

Note that we do not work with the LBL travel-times directly, instead applying the smoothing algorithm to the least-squares computed x, y fixes. In principle, a modified Kalman filter/smooth could be applied to the travel times directly, but the spherical navigation problem is nonlinear and the potential gains associated with such an increase in complexity are unclear. Also note that before the fix is computed, the travel-times are cleaned of various LBL pathologies such as multipath and surface bounce [5].

The linear process model employed in our smoother is a simplified approximation to the full 6 degree of freedom non-linear vehicle dynamics; however, the model captures the salient characteristics of the actual dynamics.

We assume depth information provided by an on-board pressure sensor is accurate enough to allow reduction of the 3-dimensional navigation problem onto the horizontal plane. That is, only the x and y components of each navigation fix are passed through the smoother. The vehicle dynamics are modeled as a two-degree-of-freedom damped mass whose damping characteristics are linear, but dependent on instantaneous heading. Vehicle thrust is modeled as a force applied along the axis of instantaneous heading and proportional to the net thruster command in the forward direction. The heading measurement is treated as an independent variable, thus no dynamics are associated with the rotation of the model.

This latter simplifying assumption is justified by the difference in bandwidth between heading measurements and the LBL fixes, and by the relatively noise-free nature of the former compared to the latter. All attitude measurements and depth are sampled at

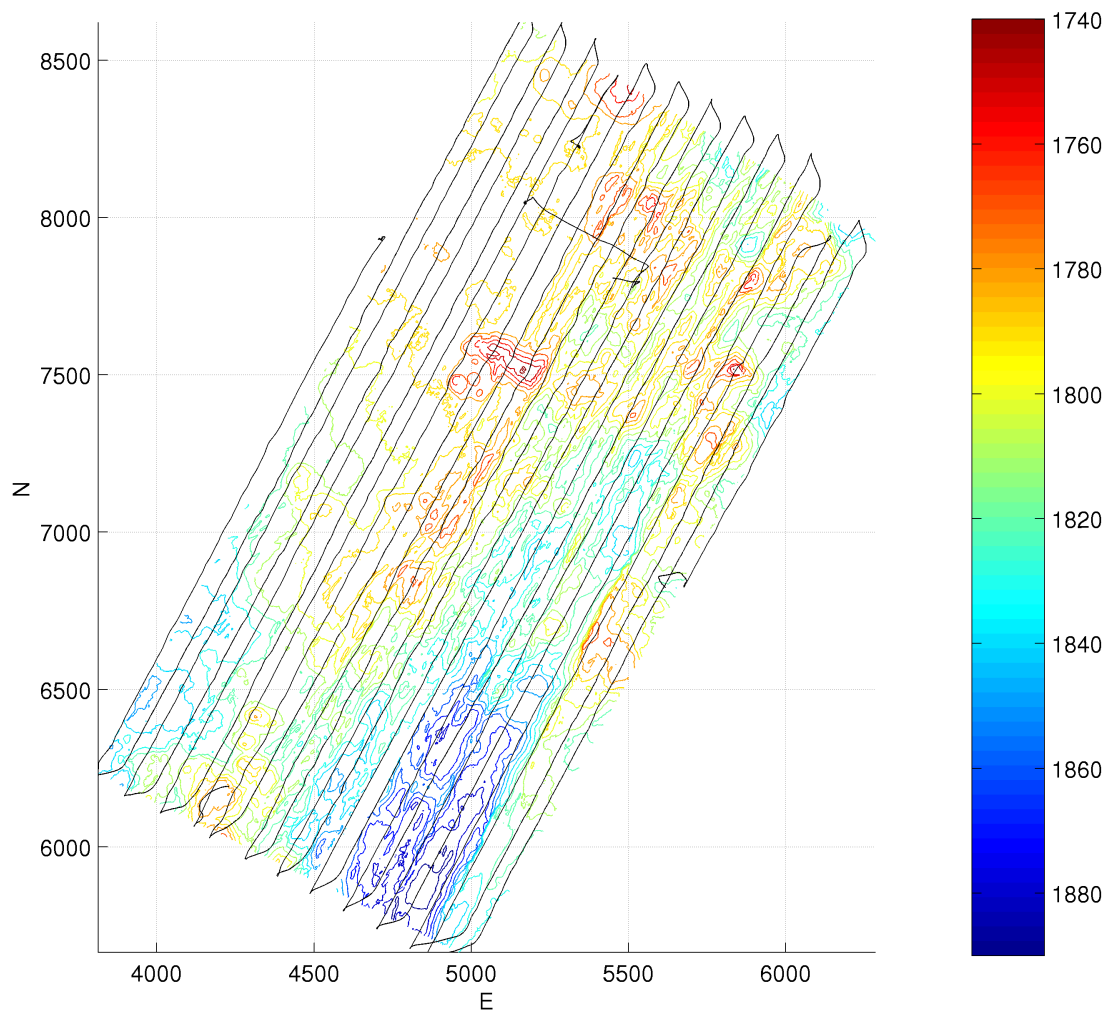


Figure 4: Vehicle trajectories for ABE-74, ABE-75, and ABE-76 superimposed over contours of the Explorer Ridge survey site. Contours are shown in intervals of 10 m.

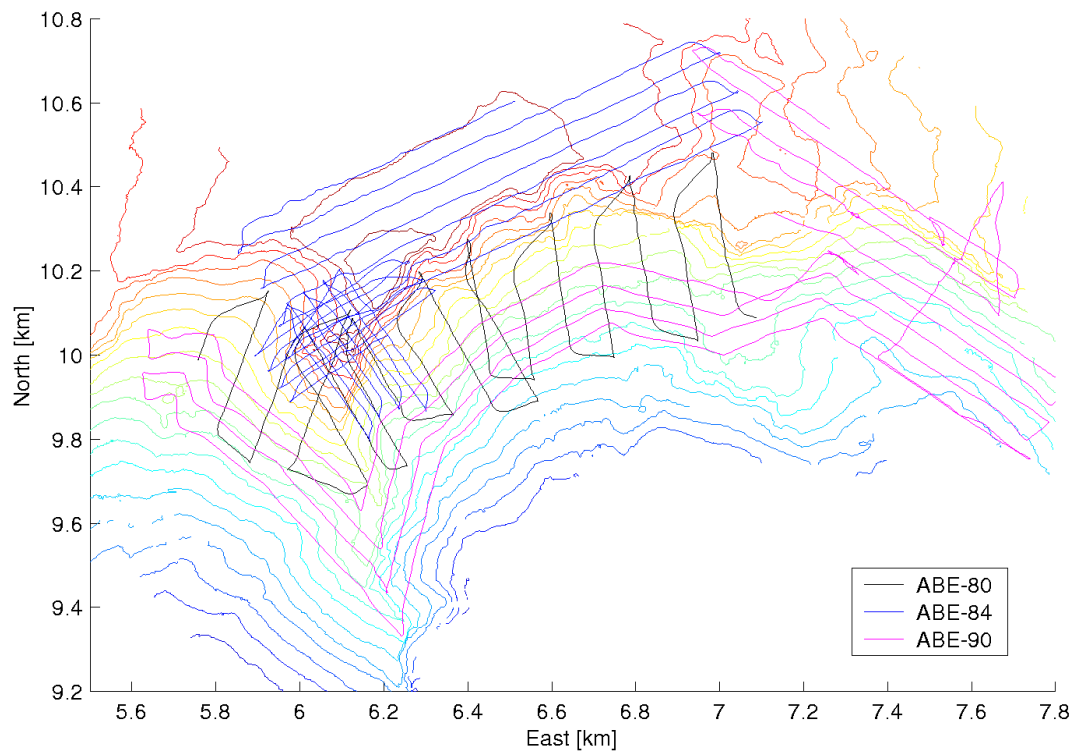


Figure 5: Selected tracklines flown by ABE over the course of 16 dives at the Lost City vent site shown superimposed over contours from the final map. Lost City itself is visible as a set of pinnacles at the top of the central ridge, just south of the summit plateau. Contours are shown at intervals of 25 m, with 100 m contours shown in bold. The depth in the figure ranges between 750 m at the summit to the deepest contour at 1300 m.

1 Hz. The LBL cycle runs at 0.1 Hz. The measured heading is of course subject to noise; however, it is the filtered average of a flux-gate compass and rate gyro, and is thus a high bandwidth, low noise measurement.

Current was observed to exert considerable influence over vehicle dynamics at the Lost city site, and to a lesser extent at Explorer Ridge. Under the assumption that the current is a slowly varying velocity source defining a moving frame within which the vehicle dynamics can be considered unaltered relative to an inertial frame, the current frame velocity $\mathbf{v}_c = \begin{bmatrix} u_c \\ v_c \end{bmatrix}$ is simply additive to velocities expressed in the LBL frame.

The simplified vehicle dynamics can then be expressed as

$$\mathbf{M} \begin{bmatrix} \ddot{x} \\ \ddot{y} \end{bmatrix} + \mathbf{D}(\psi) \begin{bmatrix} \dot{x} \\ \dot{y} \end{bmatrix} = \mathbf{B}(\psi)\tau_u + \mathbf{D}(\psi)\mathbf{v}_c \quad (1)$$

where

$$\begin{aligned} \mathbf{M} &= \begin{bmatrix} m & 0 \\ 0 & m \end{bmatrix} \\ \mathbf{D} &= \begin{bmatrix} b_x \sin^2 \psi + b_y \cos^2 \psi & (b_x - b_y) \sin \psi \cos \psi \\ (b_x - b_y) \sin \psi \cos \psi & b_x \cos^2 \psi + b_y \sin^2 \psi \end{bmatrix} \\ \mathbf{B} &= \begin{bmatrix} \sin \psi \\ \cos \psi \end{bmatrix} \end{aligned}$$

In the above, x and y are coordinates relative to the LBL net. The independent variable ψ represents the instantaneous heading of the vehicle. Under the assumption of no heading dynamics, ψ becomes simply a function of time and the above is immediately seen to be a time-dependent linear system model in state space form. The variable τ_u represents thrust applied in the forward direction; it is transformed into the LBL frame via $\mathbf{B}(\psi)$. The variables m , b_x , and b_y denote vehicle mass, forward drag, and lateral drag respectively. Our algorithm employs a discretized version of eq. (1).

The derivation of the drag matrix $\mathbf{D}(\psi)$ follows from the modeling approximations that the vehicle is axially symmetric with no hydrodynamic cross-coupling between axes, that body lift is negligible, and that the vehicle operates in a narrow enough

regime to approximate the drag forces as varying linearly with velocity.

The model parameter values used are given in Table 1. Vehicle mass was chosen to match the ABE's flooded mass, but does not include the effects of added mass. No recent data are available for vehicle drag; the values for b_x and b_y were chosen heuristically.

Table 1: ABE model parameter values

Symbol	Value	Units	Parameter
m	600	kg	vehicle mass
b_x	43	kg/s	forward drag
b_y	300	kg/s	lateral drag

Unknown current was assumed to dominate model uncertainty. Current velocities on the order of 0.1 m/s were observed around the Lost City site. This gives at least some basis for selecting an a priori model error covariance estimate \mathbf{Q} . We found

$$\mathbf{Q} = \begin{bmatrix} \sigma_{u_c}^2 & \sigma_{u_c}\sigma_{v_c} \\ \sigma_{u_c}\sigma_{v_c} & \sigma_{v_c}^2 \end{bmatrix} = 0.01 \begin{bmatrix} 1 & 0.5 \\ 0.5 & 1 \end{bmatrix} \quad (2)$$

to give results roughly consistent with the estimated model uncertainty computed by the smoother.

The nature of the noise of the computed LBL fixes is difficult to determine analytically. Empirically, the task is complicated by the differing noise properties of the LBL net as a function of position and by lack of suitable calibration data. To generate an a priori estimate of LBL noise covariance, we computed the covariances of fixes generated during the short period in each dive following descent when ABE executes a compass calibration routine by rotating slowly above a fixed point on the bottom, still tethered to its descent weight. The computed covariances for the Lost City LBL net are given in Table 2.

Figure 6 shows a closeup of the smoothed vehicle trajectory from ABE-82 in x - y coordinates. The red crosses are the original real-time fixes. The green trajectory is the output of the filter, the first stage of the RTS smoother. The blue trajectory is the output of the smoother. The jumps in the filter output indicate the effect of the unknown current. The magenta

Table 2: LBL Noise Covariance

Covariance	Value	Units
σ_x^2	2.0	m ²
σ_y^2	1.2	m ²
$\sigma_x \sigma_y$	-0.2	m ²

vectors show the current velocity field (scaled 10×) required to create the smoothed trajectory from the filtered one. As was the case for all dives over Lost City, a roughly South-tending current is evident.

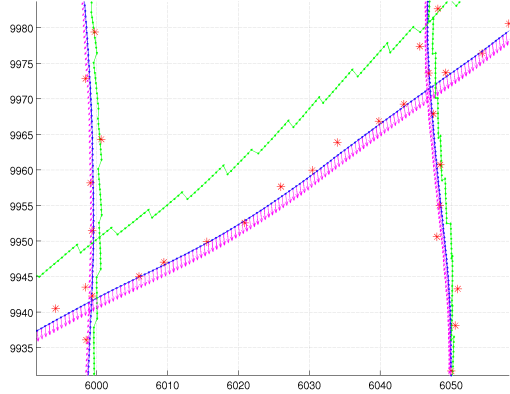


Figure 6: Real-time LBL fixes (red), filter output (green), smoother output (blue), and current estimate (magenta). The large offset and jagged shape of the filter stage output result from the influence of the unknown current. In a transverse current, the vehicle will move laterally as well as forward.

6 Multibeam Sonar Post Processing

After recovery, the digitized in-phase and quadrature sound pressure signals from each stave of the SM 2000 head are downloaded from the SM 2000 stack aboard ABE for post-processing. The entire procedure, from raw sonar data to finished map, can be completed in

less than 4 hours, meaning that bathymetric maps from one dive are available to plan the next or aid in other activities soon after recovery. Storing completely unprocessed data during the survey gives us tremendous processing flexibility in beamforming and bottom detection at the cost of increased storage requirements. The post-processing steps are shown schematically in Figure 7.

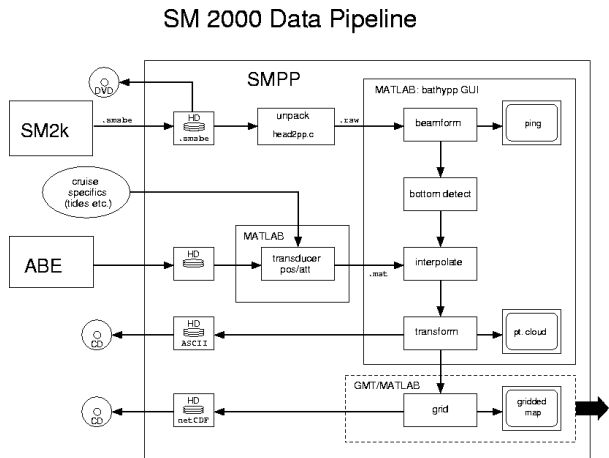


Figure 7: Post-processing schematic

Once stored on the post-processing machine, the raw sonar data is saved to DVD. Dives typically produce between 1.5 GB and 3.0 GB of sonar data depending on sonar settings and dive duration. After storage, the data are unpacked into .raw format. This binary format is compatible with the Simrad Mesotech topside unit. The data then enters the MATLAB graphical user interface (GUI) shown in Figure 8. The GUI is a front-end for a set of m-file routines that beamform the data, detect the bottom along each beam while rejecting questionable returns, interpolate vehicle position and attitude data onto the timebase of the pings, and transform the ranges and angles of each return into global coordinates. This final step produces a point cloud of accepted returns.

The bottom detection algorithm employed simply finds the maximum return along each beam. A threshold filter then rejects returns whose amplitude

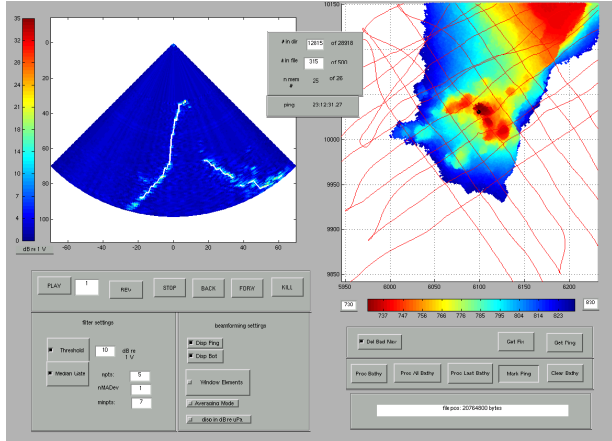


Figure 8: MATLAB graphical user interface (GUI) for bathymetry generation. The left window shows a beamformed sonar image with the white line indicating the results of bottom detection. The highlighted spire, named Poseidon, is 60 m tall and is the largest at the Lost City site. The right window shows a point cloud of accepted returns, with returns from the selected ping highlighted. The vehicle tracklines are overlaid in red. The various menus, buttons and, editable fields control the processing and provide on-the-fly access to the most commonly altered processing parameters.

falls below a user-defined threshold. Finally, a median filter is applied to the remaining points to eliminate flyers. All filters can be tuned on-the-fly or disabled.

The GUI acts primarily as a wrapper for a set of m-file bathymetry processing functions developed by the authors and Dr. Dezheng Chu of WHOI, but it implements several other features which improve a user’s ability to identify and correct problems in the data. The GUI allows users to beamform and bottom-detect alongside the corresponding bathymetry. Pings indexed by their position within a directory or file of raw data can be viewed by their index and the corresponding returns within the point cloud highlighted, or users can select returns within the point cloud and call up the corresponding sonar image. Problematic data can be reprocessed or eliminated altogether without affecting other processed

data.

7 Maps

Following the generation of a point cloud, the accepted sonar returns are interpolated onto a regular grid and plotted as two-and-a-half-dimensional surfaces of the form $z = f(x, y)$, although an explicit functional form is never computed. This procedure reduces some of the noise inherent in the survey process, by essentially low-passing the point cloud. The grid spacing and interpolation method are, to some extent heuristic choices, but should be based on a combination of navigational accuracy and sonar resolution. We found that we can reliably grid data on a 2 m square grid using a gridding technique that applies a Gaussian weighting to points within a specified radius of each grid node. At this resolution, the maps are visually free of survey artifacts, and features on the order of meters are well resolved. Figures 9 and 10 show bathymetric maps of the survey area at Explorer Ridge and a close-up of the Magic Mountain vent field. These maps represent a two-order-of-magnitude improvement in resolution over multibeam bathymetry collected from the ship and are of sufficient resolution to study outcrop-scale geology [1].

Two-and-a-half-dimensional surfaces such as that shown in Figures 9 and 10 are not complete representations of the three-dimensional surfaces they are meant to approximate. For relatively flat terrain, the distinction is immaterial; however, steeply sloped regions will fall into too few grid cells to resolve the small-scale features of their walls. This effect is evident along the cliff face on the Western edge of Figure 10. Overhangs cannot be resolved at all. Down-looking bathymetric surveys gather little data from steeply sloped faces, so often the collected data is adequately represented on a horizontal grid. The side-looking surveys ABE conducted at the Lost City site; however, provided a resolution on sloped faces comparable to that of a down-looking survey on flat terrain. To capitalize on data from the side-looking surveys, we gridded returns from these surveys on sloped grids roughly aligned with bathymetry. One

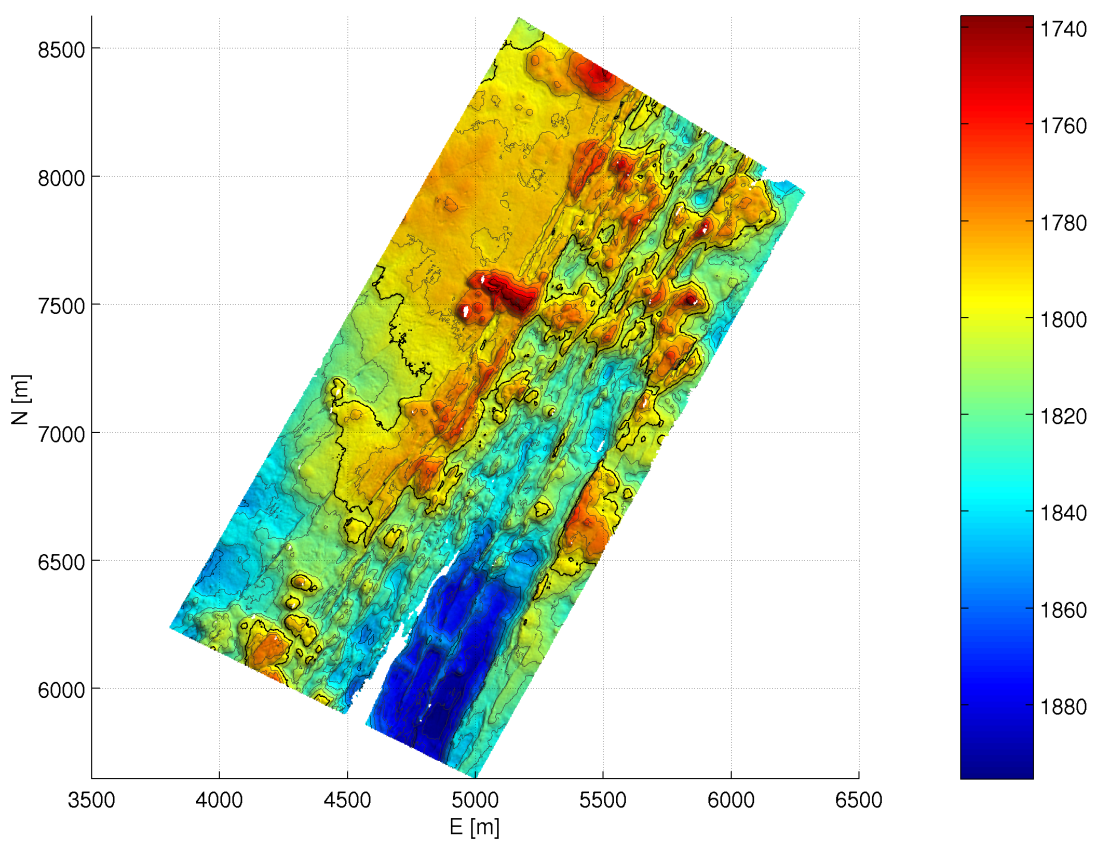


Figure 9: Explorer Ridge SM 2000 survey area bathymetry.

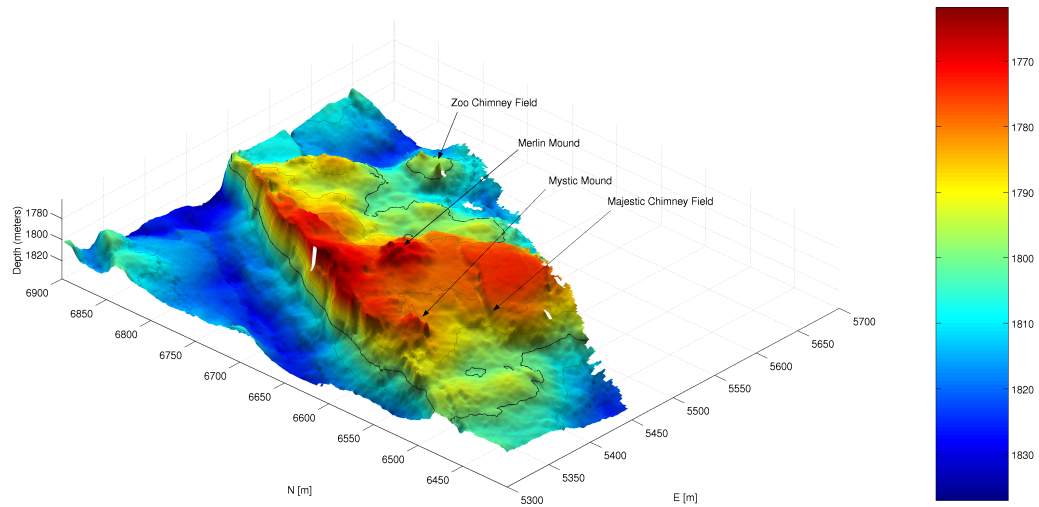


Figure 10: Close-up bathymetry of the Magic Mountain vent site gridded at 2 m. Vent fields were discovered on the mounds indicated by the arrows by ROV ROPOS on later dives [2]. Two 15 m spires are visible in the NE corner of the map.

such map, shown in Figure 11 shows the cliff face East of Lost City gridded on a cylindrical surface. We are working on techniques to combine bathymetry collected during down-looking and side-looking surveys to produce true three-dimensional surfaces while retaining the favorable low-pass characteristic inherent in gridding techniques.

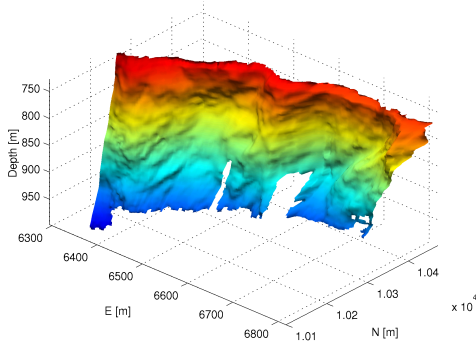


Figure 11: Side-looking bathymetry of the cliff face East of Lost City collected during ABE-81. The data are gridded on a cylindrical grid defined such that its radius roughly inscribes the cliff itself.

8 Error Analysis

It is inherently difficult to gauge the accuracy of bathymetry generated with ABE without the benefit of ground-truth. Navigation and attitude biases are typically evident as along-track artifacts, but become obscured at resolutions nearing that of the sonar. We believe we are operating near this threshold.

Close inspection of point clouds generated by successive passes over featured regions, in particular Lost City itself, revealed small x, y navigation offsets between 1 and 5 m between successive passes. When averaged together, points from multiple passes tend to smooth out small-scale features visible in single passes. Figure 12 shows part of the point cloud generated over a small section of Lost City during ABE-84. Points from three separate partially-overlapping

passes over the same area are shown. Single passes show good correspondence between neighboring returns, except on steep edges which tend to be ambiguously resolved. In contrast, points from different passes show reduced correspondence.

Assuming that the navigation offsets inferred from point clouds like that in Figure 12 are approximately zero-mean over the course of an entire dive, a map of regions covered by multiple passes will be accurate in a low-passed sense. That is, well resolved features will be accurately placed in global coordinates, but smaller-scale features that may be visible in a map generated from a single pass will be obscured. Thus maps generated from single passes will exhibit a higher resolution and concurrently a lower accuracy than maps generated from multiple passes and gridded on the same scale. However, single passes are more prone to noise originating from the bottom detection process.

We studied the variance of the point cloud generated by ABE-84 over Lost City as the number of passes whose points were included was increased. A total of 14 passes were made over the region studied. A measure of the variance was computed by sorting the returns into square bins 2 m wide, and then computing the variance of the points in each bin. This method is not free of correlation with the actual topology; however, it does provide some measure of the correspondence between neighboring points. The bin size was chosen to match the grid spacing of our maps. Figure 13 shows the increase in average standard deviation of the bins as the number of passes included increases.

The apparent asymptotic behavior of the mean variance may represent a indication of the magnitude of navigation errors between tracklines although it is difficult to separate this effect out from variance introduced by the bathymetry itself (i.e. regions with very rough topography will exhibit high binned variance regardless of navigational accuracy). Thus the inferred asymptote likely represents a combined function of navigational accuracy and of the roughness of the actual bathymetry on a 2 m scale. Noise inherent in the bottom detection process also plays a role by setting a lower bound on the binned variance. Analysis of returns collected over nearly flat bottom at the

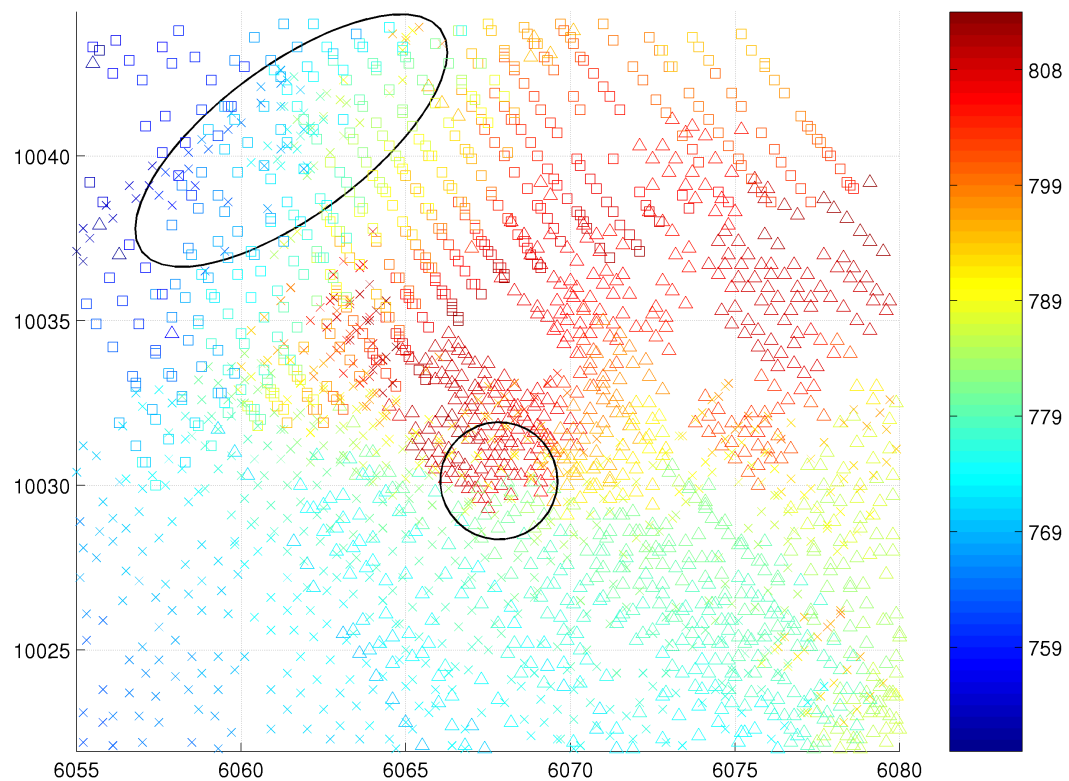


Figure 12: Point cloud generated from three passes, with points from each pass indicated by different symbols. Points are color-coded by depth. The ellipse highlights a region of lateral (navigation) offset between points from two tracklines. The circle indicates a region of sharp relief and correspondingly ambiguous bottom detection.

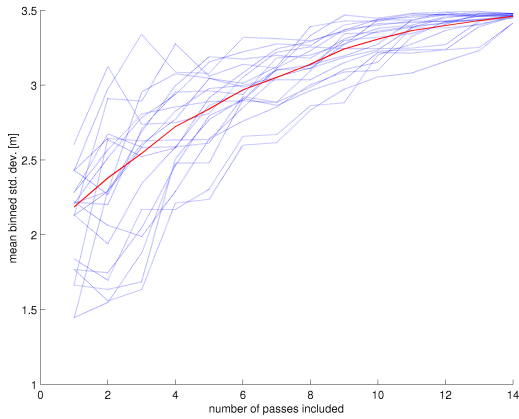


Figure 13: Average binned variance of the point cloud as a function of the number of passes included. Twenty random permutations of the order of inclusion are shown as the blue dotted curves. These were averaged together to produce the red curve.

landing site for ABE-84 indicated an average standard deviation of 0.2 m in depth across all beams although presumably this figure is larger in the rougher terrain of the region studied.

9 Conclusion

Using distinct survey strategies we were able to produce very high resolution (2 m) bathymetric maps of two sites. At the Lost City site, the particularly challenging topography required the design of side-looking surveys. The results demonstrate the potential of AUVs to collect micro-bathymetry in varied terrain on a scale not attainable from surface vessels and prohibitively costly for ROVs and piloted submersibles.

With further improvements in navigation, we expect to improve the resolution of bathymetric maps generated with ABE. Currently we conduct surveys such that sonar resolution slightly surpasses that of the navigation.

Acknowledgments

The authors would like to thank Drs. Robert Embley, Edward Baker and William Chadwick (Explorer Ridge), and Drs. Deborah Kelley and Jeffrey Carson (Lost City) for giving us the opportunity to showcase ABE’s abilities as part of their programs. We would also like to acknowledge Dr. Dezhong Chu for his multibeam processing code and advice. Our thanks go to Capt. Glenn Gomes and the crew of the R/V Thomas G. Thompson (Explorer Ridge) and to Capt. Gary Chiljean and the crew of the R/V Atlantis (Lost City) for their flawless launches and recoveries of ABE. Finally we would like to acknowledge the dedication and work of Dr. Albert Bradley (Co-P.I., ABE), Rod Catanach (mechanical), Alan Duester (electrical), Eddie Scheer (SM 2000 software), and Keith Von Der Heydt (SM 2000 software) in operating, maintaining, and upgrading ABE. Work at Explorer Ridge was supported under the NOAA Ocean Exploration Program (NA17RJ1223). Work at Lost City was supported by the National Science Foundation (OCE-137206). The SM 2000 multibeam sonar was purchased through grants provided by the NOAA Office of Ocean Exploration (NA16RP2611) and the Comer Foundation. WHOI contribution number 10979.

References

- [1] J. Carson. Personal Communication, May 2003.
- [2] R. Embley. Submarine Ring of Fire - Summary of Year One at Explorer Ridge, Dec 2 2002. oceanexplorer.noaa.gov/explorations/02fire/logs/yr_sum/yr_sum.html.
- [3] Kongsberg Simrad Mesotech LTD. *SM 2000 Multibeam Imaging Sonar*. www.simrad.ca.
- [4] C. Wunsch. *The Ocean Circulation Inverse Problem*. Cambridge University Press, 1996.
- [5] D. Yoerger, A. Bradley, M.-H. Cormier, W. Ryan, and W. B. Fine-Scale Seafloor Survey in Rugged Deep-Ocean Terrain with an Autonomous Robot. In *IEEE ICRA*, 2000.

- [6] D. R. Yoerger, A. M. Bradley, and B. B. Walden. The Autonomous Benthic Explorer (ABE): An AUV Optimized for Deep Seafloor Studies. In *Proceedings of the Seventh International Symposium on Unmanned Untethered Submersible Technology (UUST91)*, pages 60–70, Durham, NH, 1991.